International Journal of Biological Macromolecules 272 (2024) 132883

Contents lists available at ScienceDirect

International Journal of Biological Macromolecules

journal homepage: www.elsevier.com/locate/ijbiomac

A promising eco-sustainable wound dressing based on cellulose extracted from *Spartium junceum* L. and impregnated with *Glycyrrhiza glabra* L extract: Design, production and biological properties

V. Sallustio [a], M. Rossi [a,b], M. Mandrone [c], F. Rossi [d,e], I. Chiocchio [c], T. Cerchiara [a,*], E. Longo [f], M. Fratini [g], L. D'Amico [h], G. Tromba [f], E. Malucelli [d], M. Protti [i], L. Mercolini [i], A. Di Blasio [j], M. Aponte [j], G. Blaiotta [j], A. Abruzzo [a], F. Bigucci [a], B. Luppi [a], C. Cappadone [d]

[a] *Drug Delivery Research Lab., Department of Pharmacy and Biotechnology, Alma Mater Studiorum, University of Bologna, Via San Donato 19/2, 40127 Bologna, Italy*
[b] *Center for Applied Biomedical Research (CRBA), Alma Mater Studiorum, University of Bologna, Via Massarenti 9, 40138 Bologna, Italy*
[c] *Pharmaceutical Botany Lab., Department of Pharmacy and Biotechnology, Alma Mater Studiorum, University of Bologna, Via Irnerio 42, 40127 Bologna, Italy*
[d] *Pharmaceutical Biochemistry Lab., Department of Pharmacy and Biotechnology, Alma Mater Studiorum, University of Bologna, Via San Donato 19/2, 40127 Bologna, Italy*
[e] *CRMBM, CNRS, Aix Marseille University, 13385 Marseille, France*
[f] *Elettra-Sincrotrone Trieste S.C.p.A 34149, Basovizza, Trieste, Italy*
[g] *CNR-Nanotec (Roma unit) c/o Department of Physics, La Sapienza University Piazzale Aldo Moro, 5-00185 Rome (Italy) & IRCCS Fondazione Santa Lucia, Via Ardeatina, 306-00179 Rome, Italy*
[h] *Department of Physics, University of Trieste, Trieste, Italy*
[i] *Pharmaco-Toxicological Analysis (PTA Lab.), Department of Pharmacy and Biotechnology, Alma Mater Studiorum—University of Bologna, Via Belmeloro 6, 40126 Bologna, Italy*
[j] *Department of Agricultural Sciences, University of Naples "Federico II", 80055 Portici, Italy*

ARTICLE INFO

Keywords:
Glycyrrhiza glabra L.
Spanish broom
Natural extract
Wound dressing
Ethosomes
Wound healing

ABSTRACT

Glycyrrhiza glabra extract is widely known for its antioxidant and anti-inflammatory properties and can improve the wound healing process. The aim of this work was to shorten the time of the healing process by using an eco-sustainable wound dressing based on Spanish broom flexible cellulosic fabric by impregnation with *G. glabra* extract-loaded ethosomes. Chemical analysis of *G. glabra* extract was performed by LC-DAD-MS/MS and its encapsulation into ethosomes was obtained using the ethanol injection method. Lipid vesicles were characterized in terms of size, polydispersity index, entrapment efficiency, zeta potential, and stability. In vitro release studies, biocompatibility, and scratch test on 3T3 fibroblasts were performed. Moreover, the structure of Spanish broom dressing and its ability to absorb wound exudate was characterized by Synchrotron X-ray phase contrast microtomography (SR-PCmicroCT). Ethosomes showed a good entrapment efficiency, nanometric size, good stability over time and a slow release of polyphenols compared to the free extract, and were not cytotoxic. Lastly, the results revealed that Spanish broom wound dressing loaded with *G. glabra* ethosomes is able to accelerate wound closure by reducing wound healing time. To sum up, Spanish broom wound dressing could be a potential new green tool for biomedical applications.

* Corresponding author.
E-mail addresses: valentina.sallustio2@unibo.it (V. Sallustio), martina.rossi12@unibo.it (M. Rossi), manuela.mandrone2@unibo.it (M. Mandrone), francesca.rossi105@unibo.it (F. Rossi), ilaria.chiocchio2@unibo.it (I. Chiocchio), teresa.cerchiara2@unibo.it (T. Cerchiara), elena.longo@elettra.eu (E. Longo), michela.fratini@cnr.it (M. Fratini), lorenzo.damico@elettra.eu (L. D'Amico), giuliana.tromba@elettra.eu (G. Tromba), emil.malucelli@unibo.it (E. Malucelli), michele.protti2@unibo.it (M. Protti), laura.mercolini@unibo.it (L. Mercolini), annadiblasio27@gmail.com (A. Di Blasio), aponte@unina.it (M. Aponte), blaiotta@unina.it (G. Blaiotta), angela.abruzzo2@unibo.it (A. Abruzzo), federica.bigucci@unibo.it (F. Bigucci), barbara.luppi@unibo.it (B. Luppi), concettina.cappadone@unibo.it (C. Cappadone).

https://doi.org/10.1016/j.ijbiomac.2024.132883
Received 29 November 2023; Received in revised form 31 May 2024; Accepted 2 June 2024
Available online 3 June 2024

1. Introduction

Integral skin is the human body's first barrier that protects against toxins and pathogens. Moreover, it prevents excessive water loss and performs other homeostatic functions [1,2]. However, the skin may be affected by dermatological inconveniences such as burns, injuries, necrosis, exudates, and acute and chronic wounds, which the uncorrected treatment may lead to serious complications, including physical incapacities and death [3]. For this reason, in the last years, considerable attention has been paid to developing innovative and functional dressings able to promote wound healing. The healing process is characterized by a complex and dynamic series of events involving four key phases, namely, hemostasis, inflammation, proliferation, and remodeling. Currently, many wound dressings, which are prepared with different biomaterials such as cellulose, starch, chitosan, and polyurethane, have been developed to restore skin integrity by providing ideal conditions for wound healing. These include a moist environment, protection from possible infections, absorption of exudates, and exchange of oxygen and nutrients [4,5]. Taking into account these requirements for the development of effective wound dressings, Spanish broom fabric characterized by an high cellulose content is one of the most appropriate biomaterials owing to its physico-chemical and mechanical properties, rendering it flexible, soft to the touch, and easy to handle [6,7]. Spanish broom (*Spartium junceum* L.) plant belongs to the Leguminosae family and its natural bast fibres are extracted from the plant's stem. The availability, renewability, and cleaner and more resilient cultivation of Spanish broom makes it highly eco-friendly and sustainable as compared to other natural fibres. However, the cellulose of Spanish broom has the disadvantage of lacking antimicrobial activity. For this reason, Spanish broom cellulose dressings can be specifically impregnated with nanocarriers for the release of various bioactive compounds in the treatment of skin wounds [7–10].

Glycyrrhiza glabra root extract, which is rich in triterpenoid saponins and phenolic compounds, presents a great potential application for the treatment of skin injuries and wounds since it possesses several pharmacological properties, such as antioxidant, anti-inflammatory, and antimicrobial activity [11,12]. To restore the skin functionality in case of a wound, topical administration of anti-inflammatory and antioxidant extracts is required to inhibit the inflammatory cascade and allow the repair of tissue damage. For this purpose, encapsulation of bioactive compounds like phenolic compounds in nanocarriers such as liposomes, niosomes, ethosomes, transferosomes, cubosomes, and their derivates, is highly desirable because of many advantages, including direct availability at the target site as well as avoidance or reduction of side effects [1,13]. Among vesicular nanosystems, phytosomes and ethosomes have become promising drug delivery systems for skin wounds due to their biocompatibility, safety, and ability to be directly applied to the wounds. Hence, it is interesting and attractive to develop a natural wound dressing able to protect skin wounds thanks to the Spanish broom fabric and improve the healing process due to the presence of nano-encapsulated extract.

In the present work, *G. glabra* extract was characterized by HPLC-DAD-MS/MS and then encapsulated into ethosomes to protect phenolic compounds. Ethosomes were prepared by the ethanol injection method, and the physico-chemical properties of the vesicles, such as size, particle size distribution, zeta potential, encapsulation efficiency, stability on storage, and in vitro release studies were evaluated. In addition, in vitro cell viability was evaluated through resazurin metabolic assay on 3T3 fibroblasts. Antioxidant and anti-inflammatory activities were then assessed by fluorescence microscopy analysis. To prepare an eco-sustainable wound dressings, loaded vesicles were sunk into Spanish broom dressings. Moreover, the structure of Spanish broom dressings and their ability to absorb wound exudate were characterized by Synchrotron X-ray phase contrast microtomography (SR-PCmicroCT). Finally, the scratch test was performed to evaluate the wound healing properties of the Spanish broom dressing.

2. Materials and methods

2.1. Materials

Methanol, ethanol, gallic acid, and L-α-phosphatidylcholine from egg yolk were purchased from Sigma-Aldrich (Milan, Italy). Folin-Ciocalteu reagent was sourced from Titolchimica (Pontecchio Polesine, Italy). Phosphate buffer solution at pH 7.4 (PBS) contained 2.98 g/L $Na_2HPO_4x12\ H_2O$, 0.19 g/L KH_2PO_4, 8 g/L NaCl. Sodium phosphate dibasic anhydrous, sodium phosphate monobasic anhydrous, and RPMI 1640 were purchased from Sigma-Aldrich Co. (St. Louis, MO, USA). Fetal bovine serum (FBS), L-glutamine (200 mM), penicillin (10,000 U/mL), and streptomycin (10 mg/mL) were purchased from Euroclone S.p.A. (Milan, Italy). Resazurin was purchased from TCI (Milan, Italy). Spanish broom dressings were provided by Prof. Giuseppe Chidichimo of Calabria University (Arcavacata di Rende, CS, Italy). Cotton gauzes were purchased from a local drugstore. For HPLC-DAD-MS/MS analysis, pure powders of the analytes (glycyrrhizin and glycyrrhetic acid) and of ursolic acid used as the internal standard (IS), as well as all chemicals and solvents for HPLC were purchased from Merck Life Science (Merck KGaA, Darmstadt, Germany). Ultrapure water (18.2 MΩ·cm) was obtained by means of a MilliQ apparatus by Millipore (Milford, USA). Stock solutions (1 mg/mL) of the analytes and the IS were prepared by dissolving suitable amounts of pure powders in methanol. Standard solutions of the analytes and the IS were obtained by diluting stock solutions with methanol and were prepared weekly. All solutions for analysis were stored protected from light in amber glass vials from Waters Corporation (Milford, USA).

2.2. Preparation of G. glabra root extract

G. glabra L. roots were gently provided by Biokyma S.r.l. (Mocaia, 44/B, 52030 Anghiari, Italy), and vouchers of the dried plant material were deposited in the Department of Pharmacy and Biotechnology, University of Bologna (via Irnerio 42, Bologna, Italy). 300 g of dried and powdered roots underwent extraction overnight using 1 L of 70 % EtOH. Subsequently, the supernatant was filtered through a Buchner funnel, and the solvent was evaporated in a vacuum concentrator (Savant SpeedVac SPD210, Thermo Fisher Scientific, Waltham, MA, USA) at 40 °C in order to yield the crude extracts. Aliquots of the extracts were stored at 4 °C until further analysis.

2.3. G. glabra root extract characterization

2.3.1. Chemical composition by HPLC-DAD-MS/MS analysis

Quali-quantitative analyses were carried out exploiting a fully validated methodology based on liquid chromatography coupled to diode array detection and tandem mass spectrometry (HPLC-DAD-MS/MS) for the determination of glycyrrhizin and glycyrrhetic acid in crude extracts from *G. glabra* roots. HPLC-DAD-MS/MS analysis was carried out by means of a Waters (Milford, MA, USA) Alliance e2695 chromatographic system with an autosampler coupled to a Waters 2998 photodiode array detector and a Waters Micromass Quattro Micro triple-quadrupole mass spectrometer, interfaced with an electrospray ion source working in positive and negative ionisation mode (ESI+/ESI-) with polarity switching. Data processing was performed using Waters MassLynx 4.1software.

The chromatographic separation was obtained by a ChromaNik (Osaka, Japan) SunShell C8 reverse-phase column (100 × 2.1 mm I.D., 2.6 μm particles), kept at room temperature and equipped with a C8 guard column (3 × 2.0 mm, 2.6 μm); the injection volume was 10 μL. An automated composition gradient program managed a 2-component mobile phase composed of 0.1 % formic acid in water (component A) and 0.1 % formic acid in acetonitrile (component B), flowing at a constant rate of 0.25 mL/min: $t = 0$ min, A:B 95:5; $t = 2.5$ min, A:B 95:5; $t = 3$ min, A:B 50:50; $t = 7.5$ min, A:B 50:50; $t = 8$ min, A:B 95:5; $t = 9$ min,

A:B 95:5. DAD acquisition was carried out in the 200–400 nm wavelength range, while monitoring different wavelengths for each compound.

For MS/MS analysis, a multiple reaction monitoring (MRM) method was set up exploiting two different exclusive *m/z* transitions (one for quantitative purposes, one for identity confirmation). Parameter settings were optimised via direct infusion of individual analytes (1 μg/mL methanolic solutions) at 20 μL/min. The selected parameters obtained and used for sample analysis were: ion source voltage, 2.5 kV; ion source temperature, 130 °C; desolvation temperature, 310 °C; desolvation gas flow, 560 L/h; extractor potential, 2.8 V; collision exit potential, 1 V. MS/MS product ions were obtained using argon as the collision gas, with the collision energy set between 10 and 45 V. Scan was carried out in the m/z range 50–1000, with a duration of 0.5 s. for glycyrrhizin (823.1 → 453.3; 823.1 → 647.3), glycyrrhetic acid (469.7 → 175.5; 469.7 → 147.6) and IS (455.8 → 200.8; 455.8 → 407.0).

For HPLC-MS/MS analysis, crude extract samples were re-dissolved at the concentration of 1 μg/mL in an ethanol:water (1:1, *V*/V) mixture, filtered through a 0.2 μm membrane syringe filter and suitably diluted in a component A:component B mixture (1:1, V/V) before instrumental analysis. Sample processing and analysis were carried out in triplicate.

2.3.2. Total phenolic content (TPC)

The Folin–Ciocalteu assay was used to determine the TPC as reported in our previous work [14]. Firstly 0.2 mL of extract (1 mg/mL) was added to 1 mL of Folin–Ciocalteu's phenol reagent and, then 0.8 mL of sodium carbonate solution (7.5 % *w/v*). After 30 min in the dark, the absorbance at 750 nm was determined by UV–Vis 1601 spectrophotometer (Shimadzu, Milan, Italy). A standard curve of gallic acid (R^2 = 0.999) was used to determine the TPC. All measurements were performed in triplicate and results were expressed as gallic acid equivalent in mg/g *G. glabra* extract (mg GAE/g extract).

2.3.3. Antioxidant activity (AA)

The AA was determined by the DPPH free radical scavenging assay as reported in our previous work [14]. Briefly, various concentrations of extract (10, 20, 50, and 100 μg/mL) as well as ascorbic acid (used as standard antioxidant compound) were mixed with a solution of DPPH (0.1 mM in methanol) at room temperature. After 30 min at dark, the absorbance at 517 nm was determined spectrophotometrically using a UV–Vis 1601 spectrophotometer (Shimadzu, Milan, Italy). Methanol and DPPH solutions were used as blank solutions and controls, respectively. The test was carried out in triplicate. Results are expressed as a percentage of inhibition of the DPPH radical according to the following equation: Inhibition % = $[(A_0 - A)/A_0]$ where A_0 was the absorbance of DPPH control and A was the absorbance of the sample with DPPH.

2.3.4. Antibacterial activity

The antimicrobial activity of *G. glabra* root extract was first assessed by agar well diffusion assay following the procedure described by Balouiri et al. (2016) [15]. Briefly, serial 2-fold dilutions (from 12.0 to 0.25 mg/mL) in sterile deionized water were prepared, and 50 μL of each dilution were spotted onto aseptically made wells (6 mm of diameter) on Tryptone Soy Agar (TSA, Oxoid) medium previously seeded with about 10^6 CFU/mL of the target microorganisms: *Staphylococcus* (*S.*) *aureus* DSM799 (=ATCC 6538) and *Escherichia* (*E.*) *coli* DSM11250 (=ATCC 10536). Clear inhibitory halos surrounding the wells after a 24 h incubation period at 37 °C indicate an antimicrobial effect. Time–kill assays [16] were performed based on the minimum inhibitory concentration determined by agar well diffusion assay. Testing tubes containing Tryptone Soy Broth (TSB, Oxoid) medium and inoculated with *S. aureus* DSM799 (about 10^6 CFU/mL) were added of *G. glabra* root extract (0, 0.25, 0.5, 1.0, 2.0 and 4.0 mg/mL) and analyzed at time 0, as well as after 24 and 48 h of incubation at 37 °C by counting on TSA.

2.4. Encapsulation of G. glabra extract into ethosomes

To prepare ethosomes, the ethanol injection-sonication method reported by Liu et al. (2011) [17] with minor changes was used. Briefly, L-α-phosphatidylcholine (150 mg) was dissolved in ethanol (5 mL), while the *G. glabra* extract (15 mg) was dissolved in double-distilled water (10 mL) and mixed uniformly. The ethanolic solution of phospholipid was slowly (1 mL/min) added to the aqueous solution with a syringe under constant stirring at 700 rpm and at 30 °C. To homogenize the vesicle suspension an ultrasonic probe (Transonic T310, Elma, Germany) for 15 min was used. Unloaded ethosomes were prepared as the controls.

2.5. Characterization of ethosomes

2.5.1. Size and zeta potential measurements

Ethosomes vesicle size (VS) and their polydispersity index (PDI) were measured by PCS (photon-correlation spectroscopy) using a Brookhaven 90-PLUS instrument (Brookhaven Instruments Corp., Holtsville, NY, USA) with a He—Ne laser beam at a wavelength of 532 nm (scattering angle of 90°). The vesicle suspensions were diluted (1:500 *v/v*) in ultrapure water (18.2 MΩ cm, MilliQ apparatus by Millipore, Milford, MA, USA). The measurements were performed at room temperature with five runs for each determination. The zeta potential measurements were carried out at 25 °C on a Malvern Zetasizer 3000 HS instrument (Malvern Panalytical Ltd., Malvern, UK), after the same dilution.

2.5.2. Entrapment efficiency

The Entrapment Efficiency (EE) of ethosomes was measured by the dialysis method [18]. To evaluate the amount of bioactive compounds encapsulated into the vesicles, samples (1 mL) were purified from the non-incorporated components by dialysis (Spectra/Por® membranes: 12–14 kDa MW cut-off) in water (0.5 L) for 2 h at room temperature, refreshing distilled water after 30 min (2 L in total amount). The antioxidant activity (Inhibition %) of the samples, before and after dialysis, was measured by the DPPH assay, and the EE was calculated as a percentage of the antioxidant activity after dialysis versus that before dialysis as reported in this formula: EE% = (Inhibition % dialyzed sample/Inhibition% non dialyzed sample) x100.

2.5.3. Physical stability

The physical stability of the prepared ethosomes was evaluated by monitoring the probable changes in the size and the PDI. The samples were stored at 4.0 ± 1.0 °C in the dark to avoid extract oxidation and phospholipids hydrolysis [14]. At predetermined times (0, 1, 2, and 3 months), aliquots of the prepared ethosomes were diluted in ultrapure water (1:500; *v/v*), and the change of ethosomes size and PDI were measured by DLS as reported in section 2.5.1.

2.6. In vitro release studies

The polyphenols release studies from vesicles were carried out using a Franz-type static glass diffusion cell (15 mm jacketed cell with a flat-ground joint and clear glass with a 12 mL receptor volume; diffusion surface area = 1.77 cm^2) equipped with a V6A Stirrer (PermeGearInc., Hellertown, PA, USA). A cellulose membrane (MF-Millipore cellulose nitrate 0.22 μm, Sartorius Stedim, Biotech GmbH, Germania) was placed between the receptor and the donor compartments, and 12 mL of a mixture of 3:7 (*v/v*) ethanol/pH 7.4 buffer was used as the receptor medium. The donor compartment was filled with 0.5 mL of vesicles suspension. The systems were kept at 32.0 ± 1.0 °C under magnetic stirring (100 rpm/min). Aliquots (0.2 mL) were withdrawn at predetermined intervals, and the release medium was refilled with the same volume. The amount of polyphenols released was determined by UV–Vis spectrophotometry using the Folin-Ciocalteu method and compared with the free extract dissolution in the same medium. The polyphenol release profiles were performed in triplicate.

2.7. Preparation of Spanish broom wound dressings containing G. glabra extract-loaded ethosomes

2.7.1. Synchrotron X-ray phase contrast microtomography (SPCmicro-CT) of Spanish broom wound dressings

The morphological and structural characterization of Spanish broom in comparison with cotton dressings was performed by SPCmicro-CT at the SYRMEP (SYnchrotron Radiation for MEdical Physics) imaging beamline of Elettra synchrotron in Trieste (Italy) [19]. This imaging technique is sensitive to small phase shifts in weakly absorbing objects, overcoming the limitations of conventional absorption-based microCT [19] and thus allowing a non-invasive investigation of soft matter microstructures. The capabilities of X-ray phase-contrast tomography for non-destructive studies of the micro-architecture of soft tissues and have recently been demonstrated by several authors [20–24].

In our work, phase-contrast imaging was beneficial for imaging Spanish broom and cotton fibres with increased contrast resolution. Single macroscopic fibres were extracted from the cotton and Spanish broom based dressings and inserted inside plastic capillaries for the PCmicroCT acquisitions. Both types of fibres were imaged in dried and wet conditions using a simulated fluid wound medium (SWF). The investigations were carried out at an average energy of 19.3 keV by filtering the white/pink beam with 1.0 mm thick Silicon (Si) filter while the energy storage ring was operating at 2.0 GeV. Phase-contrast was achieved by implementing a single-distance propagation-based setup with a sample-to-detector distance of 15 cm. MicroCT scans were accomplished by rotating the capillary and collecting 1800 projections (i.e., radiographies) of the fiber. In addition to the sample radiographies, 20 flat fields (i.e., background images) and 20 dark fields (i.e. dark images) were collected at the beginning of each tomographic measurement for the subsequent image processing step. The projections were acquired with an effective pixel size of 0.9 μm using a sCMOS ORCA Flash 4.0 Hamamatsu camera (2048 pixels × 2048 pixels with physical pixel size 6.5 μm) equipped with a zoom system and coupled to a 17 μm thick GGG scintillator screen. All images were acquired with an exposure time of 100 ms. Volumetric datasets were reconstructed using the open-source software SYRMEP Tomo-Project (STP) [25]. Specifically, after conventional flat-fielding, the projections were phase-retrieved using Paganin's algorithm with a delta/beta ratio equal to 150. Then, virtual slices corresponding to the axial planes of the samples were recovered by Filtered Back Projection algorithm combined with Shepp-Logan filter. During the stage of pre-processing, possible ring artefacts were attenuated using Rivers filter available with STP software [25]. Reconstructed slices were inspected with the open-source software Fiji which was used to mask the background and compute the related statistical analysis described in the following. 3D visualizations were realized using Amira software. Furthermore, SB yarn 3D reconstruction was derived from SPCmicro-CT acquisitions performed at an average energy of 16.7 keV, an exposure time of 50 ms per projection, pixel size of 1.6 μm and sample to detector distance of 15 cm. The images were reconstructed and rendered as described above.

Thanks to SPCmicro-CT, it was possible to characterize and quantify morphological changes in fibres and bundles cross sections after the absorption of SWF. In particular, mean cross-sectional bundle areas and mean fibres areas were computed. Concerning the mean cross-sectional bundle area, reconstructed tomographic slices were masked in order to isolate bundle sections in both dry and wet samples. The mean cross-sectional bundle area was computed in both conditions, and the increment due to bundle capacity to retain SWF was derived as the ratio between wet and dry mean bundle areas. The mean fibres area quantifies the SWF up-taken by the fibres and their wickability. Reconstructed tomographic slices were masked in order to isolate fibres sections in both dry and wet samples. The fibres increment due to SWF uptake was quantified as the ratio between wet and dry mean fibres areas.

2.7.2. Impregnation of Spanish broom dressings with ethosomes

Spanish broom cellulose fibres extracted by patented DiCoDe (digestion–compression–decompression) process were used to manufacture wound dressings [7,26]. To obtain antioxidant wound dressings, the ethosomal suspensions prepared, as reported in Section 2.4 were placed onto Spanish broom dressings to favor the absorption of the vesicles by impregnation [7], the most commonly used and convenient process for depositing nanosystems on fibres [27]. Spanish broom dressings (2 × 2 cm) were uniformly wetted with 75 μL of ethosomal suspensions for 15 min. The developed dressings were then sealed in aluminum foil bags and stored at 4–8 °C until use.

2.8. Cell-viability assay

3T3 murine fibroblast cells were grown in RPMI supplemented with 10 % FBS, 2 mM L-Glutamine, 100 units/mL penicillin, and 100 μl/mL streptomycin (MICROGEM, Naples, Italy) at 37 °C in a 5 % CO_2/95 % air humidified atmosphere. To evaluate the biological effect of the different formulations, the cells were seeded in 96-well plate at the density of 10,000 cells/cm^2. The following day, different concentrations of the ethosomes (200, 100, 50, and 25 μM of extract) were tested and incubated for 24 h.

Cell viability was estimated using the colorimetric indicator resazurin. This test allows the assessment of changes in metabolic activity reflecting the cell viability by using a resazurin-based reagent. Briefly, after 24 h of treatment, the culture medium was exchanged with fresh media containing 100 μM resazurin and incubated for 4 h at 37 °C in the dark. Finally, fluorescence intensity was measured with a plate reader (EnSpire Multimode Plate Reader, Perkin-Elmer) applying a λ_{exc} of 560 nm and λ_{em} of 590 nm. The percentage reduction of AlmarBlue was normalized to that of the basal medium using the equation: F590 sample * 100/F590 basal medium.

2.9. Hemolysis assay

Human blood was obtained in accordance with the ethical standards, the Declaration of Helsinki and national and international guidelines from the Immunohaematology and Transfusion Medicine Service Bologna Metropolitan Area (Protocol number 0000816 of 23/02/2024). Erythrocytes from human blood were collected by centrifugation at 116 *g* for 15 min, and then diluted to 5 % (*v/v*) with PBS. Next, 0.5 mL of *G. glabra* root extract (0.2 mg/mL) and nanovesicle formulations were mixed with 0.5 mL of diluted red blood cells. Triton X-100 (0.1 % *v/v*) or PBS were used as a positive and negative control, respectively. Finally, samples were kept warm for 1 h at 37 °C, and then centrifuged at 8000 *g* for 5 min. The absorbance of supernatants was detected at 542 nm. The hemolysis rate of the samples was calculated by the following formula:

$$Hemolysis\ (\%) = \frac{(Sample\ abs542nm - Negativecontrol\ abs542nm) \times 100\%}{(Positivecontrol\ abs542nm - Negativecontrol\ abs542nm)}$$

2.10. Antioxidant activity

3T3 cells were seeded at a density of 30,000 cells/cm^2 in a 96-well plate. After 24 h, cells were treated with *G. glabra* root extract (0.1 mg/mL), nanovesicles and ascorbic acid solution (25 μg/mL) for 24 h. After washing in PBS, the fluorescent probe H_2DCFDA (Sigma-Aldrich, Milan, Italy) was added at the concentration of 2 μM in phenol red-free RPMI medium for additional 30 min. After washing in PBS, samples were analyzed by confocal microscopy (Nikon Eclipse TE300) using λ_{exc} of 488 nm and λ_{em} of 515 nm. Finally, the fluorescence intensity of the acquired images was measured by FIJI software.

2.11. Anti-inflammatory activity

3T3 cells were seeded at 10000 cells/cm^2 on a glass coverslip and

incubated for 24 h. In order to induce an inflammation state, a complete culture medium was replaced with a serum-free one for 6 h. Next, cells were treated for 24 h with and without 0.5 μg/mL of lipopolysaccharide (LPS) and loaded formulation in complete medium. Samples were then fixed with formalin solution (10 % in PBS) for 20 min at RT and, after washing with PBS glycine 0.1 M, permeabilizated with cold ethanol 70 % (*v/v*) for 3 min at −20 °C. After washing with PBS 1 % BSA, samples were incubated with the primary antibody (rabbit anti-NF-kB p65, 1:500, Cell signaling, Danvers, MA, USA) for 1 h at RT. After washing, secondary antibody FITC-conjugated was added (1:500, Sigma-Aldrich, Milan, Italy) for 1 h at RT. Finally, coverslips were mounted with Fluoroshield™ with DAPI (Sigma-Aldrich, Milan, Italy). Images were acquired by Nikon Eclipse TE300 confocal microscope.

2.12. Wound-healing assay by quantitative phase imaging (QPI) analysis

A square of Spanish broom dressing (area 2 cm^2) was loaded with 75 μL of extract, loaded, and unloaded vesicles. A complete absorption of the formulations was reached after 15 min. Dressing samples were then immersed in 6 mL of RPMI and incubated at 32 °C for 6 h under magnetic agitation. Finally, the dressing was removed from the medium, and the resulting suspension was centrifugated at 2000 rpm for 10 min. Finally, the supernatant was filtered through a 0.45 μM syringe filter and supplemented to obtain the final extract in a complete medium supplemented with 10 % FBS, 2 mM L-Glutamine, 100 units/mL penicillin, and 100 μl/mL streptomycin.

To assess the healing capacity of the selected dressing, 3T3 cells were seeded in a 12-well plate at a density of 35,000 cells per well and incubated until confluence was reached. The cell monolayers were then manually scraped with a p200 pipette tip and washed twice with PBS to remove cell debris. Finally, cells were treated with 1 mL of extracts prepared as described above. QPI imaging was performed with the Livecyte™ imaging system (Phase Focus, Sheffield, UK). QPI images were acquired every 60 min for 48 h, and data were analyzed with the Cell Analysis Toolbox software (Phase Focus, Sheffield, UK).

2.13. Statistical analysis

Each experiment was performed three times, and all results are shown as mean ± standard deviation (SD). Data from all experiments were analyzed using *t*-test or one-way and two-way ANOVA test and differences were deemed significant for * $p < 0.05$, ** $p < 0.01$, *** $p < 0.001$. All the graphs, calculations, and statistical analyses were performed using GraphPad Prism software version 8.0 for Windows (GraphPad Software, San Diego, CA, USA).

3. Results and discussion

3.1. G. glabra root extract characterization

Nowadays, *G. glabra* root extracts are used in pharmaceutical, cosmetic and food industries as well as in the production of functional foods and dietary supplements [28] thanks to their selective biological activities. The main bioactive components of *G. glabra* root extract are flavonoids, glycyrrhizin and its aglycone, 18β-glycyrrhetic acid, which are responsible for antioxidant, antimicrobial and, anti-inflammatory activities [29].

The ethanolic extract of *G. glabra* root used for this work and analyzed by HPLC-DAD-MS/MS had glycyrrhizin and glycyrrethic acid content of 104.94 μg/mg and 0.06 μg/mg, respectively. The TPC value of *G. glabra* extract determined by Folin-Ciocalteu method was 55.56 ± 1.15 μgGAE/ mg extract; while the antioxidant activity (AA) of 1 mg/mL solution of *G. glabra* extract measured by the DPPH assay was 86.79 ± 0.64 %. Agro-climatic conditions such as rainfall, altitude, or soil composition might influence TPC content and AA; however, values obtained for both TPC and AA are consistent with those reported by Ercisli et al. (2008) and Lim (2016) [30,31]. By agar well diffusion assay, the extract proved to be active against *S. aureus* DSM799 but not against *Escherichia coli* DSM11250 (data not shown).

According to previous studies, *G. glabra* root extract was more effective against Gram-positive bacteria than Gram-negative ones [32]. Specifically, at a concentration of 1 mg/mL, the extract produced a clear inhibition halo of about 0.4 mm against *S. aureus* DSM799 (data not shown). Time–kill assays highlighted the bactericidal activity of the extract at a concentration ≥ 1 mg/mL (Fig. 1) and that this activity is dose and time-dependent. Particularly, at concentrations of 4 and 2 mg/mL the extract was able to reduce the initial microbial load (10^6 CFU/mL) to at least 5 log CFU/mL in 48 h. In fact, in these conditions, bacterial population levels dropped below the detection limit of the method (1 log CFU/mL). A lower bactericidal activity was recorded in cultures supplemented with 1 mg/mL of extract showing a 3 log CFU/mL reduction after 48 h of incubation. However, the bactericidal endpoint has been subjectively defined as the lowest concentration at which 99.9 % of the final inoculum is killed (CLSI, 1998) [33].

3.2. Encapsulation of G. glabra extract into ethosomes

Ethosomes loaded with *G. glabra* extract were obtained by the ethanol injection-sonication method and were characterized for size, PDI, zeta potential, EE, and stability over three months. The characteristics of loaded and unloaded ethosomes are reported in Table 1. The size of ethosomes loaded with *G. glabra* extract and unloaded is below 200 nm; unloaded ethosomes present smaller mean diameters than loaded ones. The size enlargement after the extract loading process can be correlated to the encapsulation of phytochemicals in the vesicle structure. Our results are in good agreement with the literature data as reported by Sallustio et al. (2022) and Pavaloiu et al. (2020) [14,34].

The PDI values show size homogeneity of the lipid vesicular systems, particularly PDI values <0.1 indicate a homogeneous population, while values higher 0.3 show a big heterogeneity [34]. Ethosomal formulations showed low PDI values indicating a good homogeneity of the vesicles.

Regarding the zeta potential, unloaded ethosomes, as well as loaded ethosomes, are characterized by zeta potential values more negative than −30 mV, indicating good stability [35]. Generally, a negative zeta potential value is due to the presence of the phosphate functional group of phosphatidylcholine. The results are in good agreement with the literature data [14].

Entrapment efficiency (EE%) represents a crucial parameter for the evaluation of the potentiality of a delivery system. Ethosomes loaded with *G. glabra* extract showed high EE (92.37 ± 2.9 %), indicating that the preparation method was efficient and that extract loss during preparation was minimal.

3.3. Stability studies

To assess the physical stability of the loaded and unloaded lipid vesicles, changes in size and PDI were monitored at different storage periods (up to 12 weeks) at 4 °C. The size changes of unloaded and loaded ethosomes are shown in Fig. 2. The variations in size for unloaded and loaded ethosomes is <20 nm in the 12 weeks, and for this reason, both formulations could be considered stable. No relevant changes were detected with respect to PDI for ethosomes, confirming a homogeneous size distribution over the tested period. Moreover, no sedimentation was visually observed during storage, probably due to the Brownian motion and the diffusion rate, which in the case of nano-sized formulations are higher than the gravitational-induced sedimentation rate [36,37].

3.4. In vitro release studies

The polyphenols release study from ethosomes loaded with *G. glabra*

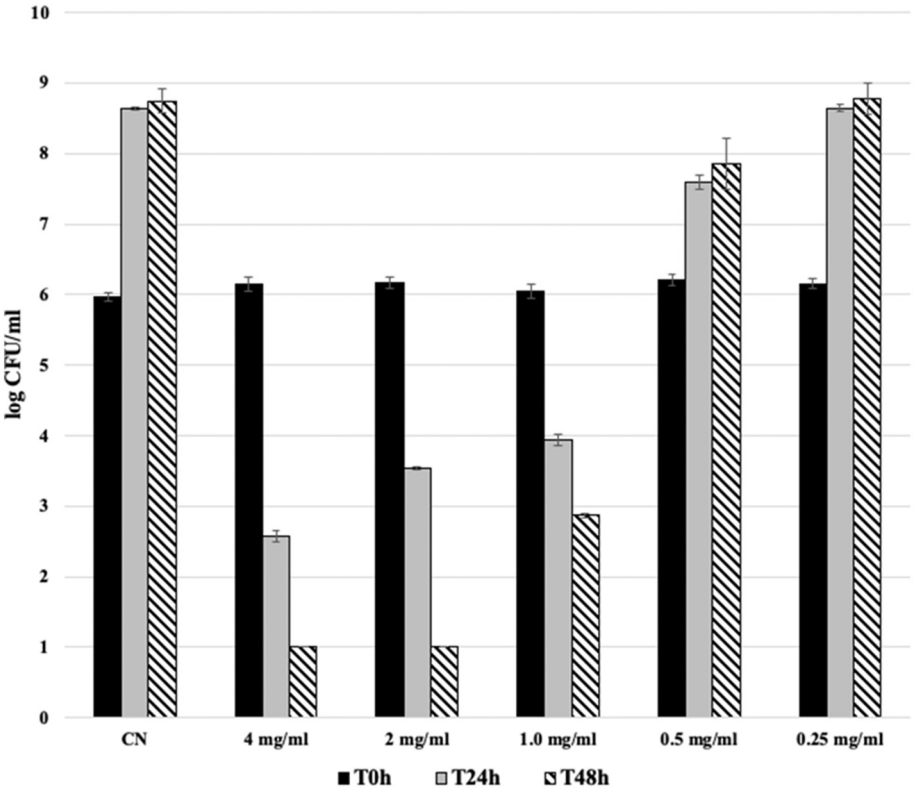

Fig. 1. Effect of five different concentrations of *G. glabra* root extract on *S. aureus* DSM799 over a 48 h using TSB medium.

Table 1
Vesicle size, PDI, ζ potential, and EE of unloaded and loaded ethosomes.

Sample	Size (nm)	PDI	ζ-potential	EE%
Ethosomes unloaded	143.95 ± 8.1	0.107 ± 0.02	−46.99 ± 1.61	–
Ethosomes loaded	165.90 ± 7.8	0.089 ± 0.003	−44.37 ± 0.73	92.37 ± 2.9

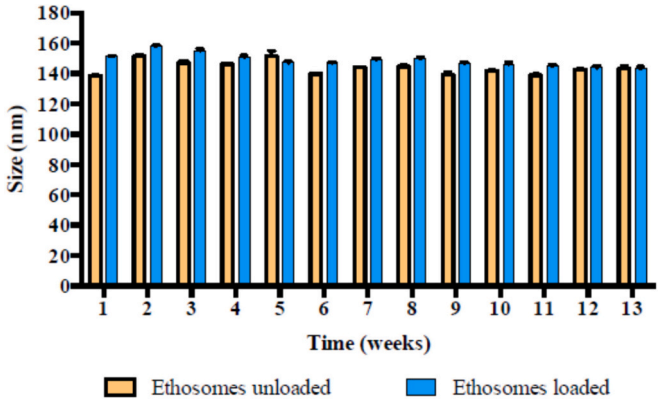

Fig. 2. Sizes of unloaded and loaded ethosomes during 12 weeks of storage at 4.0 ± 1.0 °C (Data expressed as mean ± SD, $n = 3$).

extract and the free extract solution (1 mg/mL, *G. glabra* solution) was performed in a mixture of 3:7 (*v/v*) ethanol/pH 7.4 buffer at a temperature of 32 ± 1 °C. The Folin–Ciocalteu test was used to determine the TPC released over a 24 h period. The results are shown in Fig. 3 and are expressed as the percentage of TPC released over time. The free extract exhibited a fast release with ~ 99 % TPC after 24 h. On the other hand, the

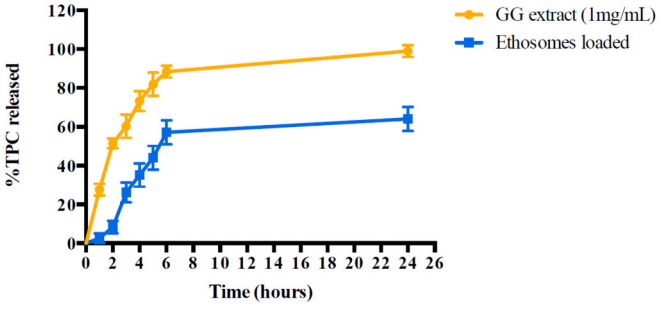

Fig. 3. *In vitro* release of TPC from loaded ethosomes and *G. glabra* extract. (Data expressed as mean ± SD, n = 3).

extract encapsulated in ethosomes showed a slow release over time, and after 24 h, the amount of TPC released was 64.08 ± 6.24 % ($p < 0.001$). The results highlighted that the release profile of polyphenols is affected by the presence of the lipid vesicles having the ability to guarantee a controlled release of the extract at the wound site, providing an intrinsic therapeutic benefit.

3.5. Biological studies

3.5.1. Cell-viability assay

A basic requirement of pharmaceutical formulations for wound healing is biocompatibility and non-toxicity on cell metabolism. To assess cell viability, the resazurin assay was performed on 3T3 fibroblasts. Fibroblasts, along with keratinocytes, represent the main cell types involved in the skin regeneration process. Treatment with the pure extract induced no toxic effect up to a concentration of 100 μg/mL, while a 30 % reduction was observed at 200 μg/mL (Fig. 4). Furthermore, even when the extract was encapsulated into ethosomes no cytotoxicity was observed, although an 80 % reduction is evident at the

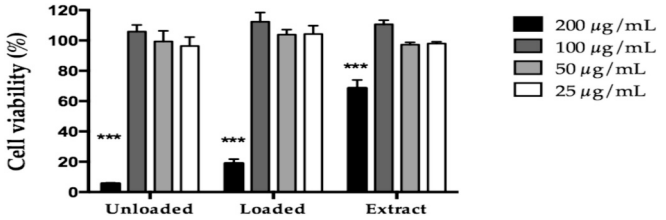

Fig. 4. Biocompatibility assay. Cells were treated with different concentrations of ethosomes and extract, respectively. After 24 h of treatment, a resazurin assay was performed. A two-way ANOVA test was performed.

highest concentration. To verify the non-toxicity of the vesicles, the unloaded ethosomes were also tested on fibroblasts, and the reduction in viability at 100 μg/mL was superimposed on the control samples.

3.5.2. Hemolysis assay

To shed more light on medical applications of *G. glabra* root extract and loaded and unloaded nanovesicle formulations, their anti-hemolytic properties were evaluated. The lower the hemolysis rate indicates the higher the hemocompatibility. The Fig. 5 shows that the hemolysis rate was <5 % for all the tested samples, which meets the national safety standards. Hence, blood compatibility makes the nanovesicles under study suitable for wound treatment.

3.5.3. Antioxidant activity

To assess the antioxidant properties of nanovesicle formulations loaded with *G. glabra* extract, cell fluorescence was analyzed through confocal microscopy after H_2DCFDA staining [38]. Representative images are shown in Fig. 6A, and the relative fluorescence intensity quantifications are reported in Fig. 6B. Interestingly, loaded ethosomes induce a marked antioxidant effect, reducing ROS levels by approximately 75 %, indicating that ethosomes are able to control oxidative process. Even *G. glabra* extract showed a significant fluorescence decrease, comparable to that obtained with the standard antioxidant Ascorbic Acid.

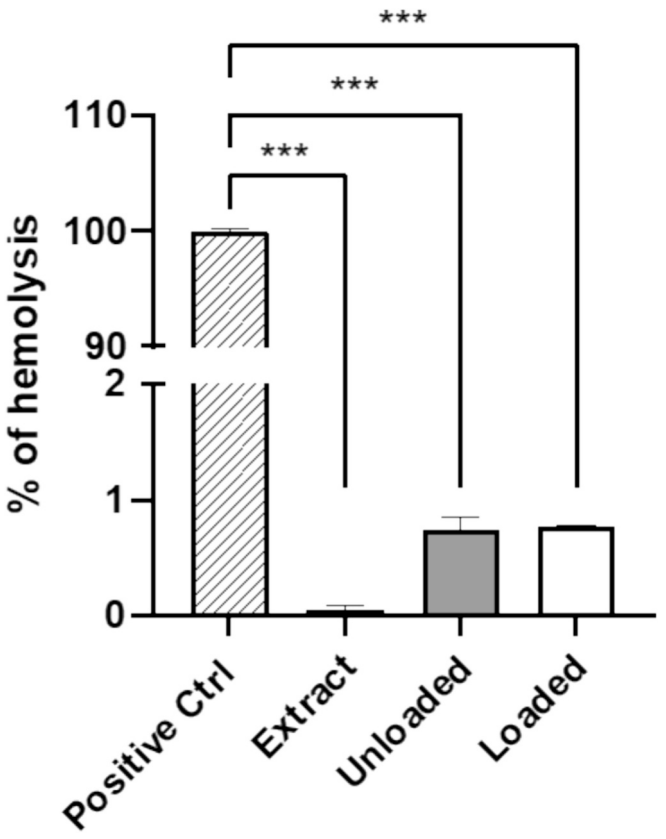

Fig. 5. Hemolysis assay. Hemolytic percentage after treatment with *G. glabra* root extract and loaded and unloaded nanovesicle formulation. Triton X-100 was used as a positive control, while PBS as negative control (bar is not reported being about 0 %).

3.5.4. Anti-inflammatory effect

It is well known that NF-kB plays a key role in the inflammatory cascade. Its inactive form resides in the cytoplasm, bound to the inhibitor IkB. After an inflammatory stimulus such as LPS treatment, IkB is phosphorylated and dissociates from NF-kB. Successively, NF-kB translocates to the nucleus, modulating the expression of inflammation target genes [39]. Our data suggest the anti-inflammatory activity for ethosomes loaded with *G. glabra* root extract (Fig. 7). In fact, the treatment of 3T3 cells determined the inhibition of LPS NF-kB transcriptional activity, preventing its nuclear translocation. On the other hand, untreated samples show a higher nuclear localization due to inflammation triggered by LPS.

3.6. Synchrotron X-ray phase contrast microtomography (SR-PCmicroCT) of Spanish broom wound dressings

Wound dressing efficiency mainly relies on the dressing's surface topography. Therefore, a morphological characterization of wound dressings architecture and its fibres arrangement and structure holds great potential in medication improvements. Indeed, these parameters greatly affect the adhesion, proliferation, penetration of the cells, and release behaviour of the bioactive molecules from the wound dressings [40]. The SWF absorption of Spanish broom and cotton dressings is affected by the fibres structure, which is characterized by variously sized pores or capillary spaces between the fibrils. This internal structure of fibres makes cellulose dressings accessible to liquids and vapours, influencing fibres wickability and absorbing capacity. In fact, the reaction of cellulose with SWF produces swelling of the fibres and a morphological change that could be appreciated at a micrometric spatial resolution thanks to SR-PCmicroCT. In particular, components of the Spanish broom and cotton, such as fiber bundles, were imaged without sectioning, staining or other destructive sample preparation procedures, with high resolution and full 3D coverage. In this context, a detailed characterization of changes induced by exudate on fibres morphology could promote the application of Spanish broom in the medical field, specifically on wound dressing development.

Figs. 8 (a) and (b) show a 3D rendering of a Spanish broom bundle. The transversal axial planes of Spanish broom and cotton before and after SWF uptake (Figures c, d, e, and f) allowed to appreciate and characterize the morphology of the two different elementary fibres. Figures g and h illustrate a 3D rendering of Spanish broom wet fibres (g) and cotton (h) extracted from their corresponding yarns.

In dry Spanish broom, the elementary fibres are densely packed in bundles (Figure c). In addition, thanks to the high resolution and the phase changes sensibility, fibres lumens can be appreciated in some of them. Upon SWF uptake, Spanish broom fibres increased their fibrous area, revealing polygonal-shaped fibrils and the presence of a well-defined lumen in their inner part (Figure d). This increment has been quantified thanks to the high sensitivity of SR-PCmicroCT. Soaked and dry fibres mean cross-sections highlighted (see Table 2) an increase of fibres area of a factor 2.18 with respect to the dry condition. Furthermore, exudate penetration among fibres decreased their packing and increased the bundle mean cross-sectional area by a factor 3.6, underlining the Spanish broom's capacity to retain exudate. In cotton, the individual fibres inside the bundle could be seen as C-shaped cells (Figures e and f), showing a dark inner lumen in both dry and soaked samples. Cotton fibres appeared less packed, and upon imbibition, their fibrous area did not considerably increase if compared to Spanish broom. In fact, soaked fibres mean cross-sections increased of a factor

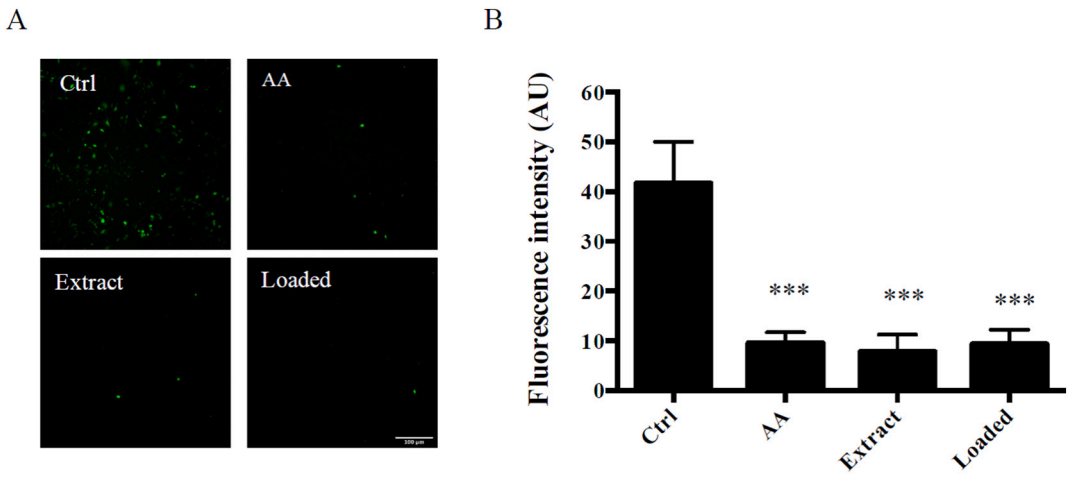

Fig. 6. Antioxidant activity. A) Representative fluorescence confocal images. B) Fluorescence intensity quantification. Oxidative stress was detected by H_2DCFDA staining after 24 h treatment.

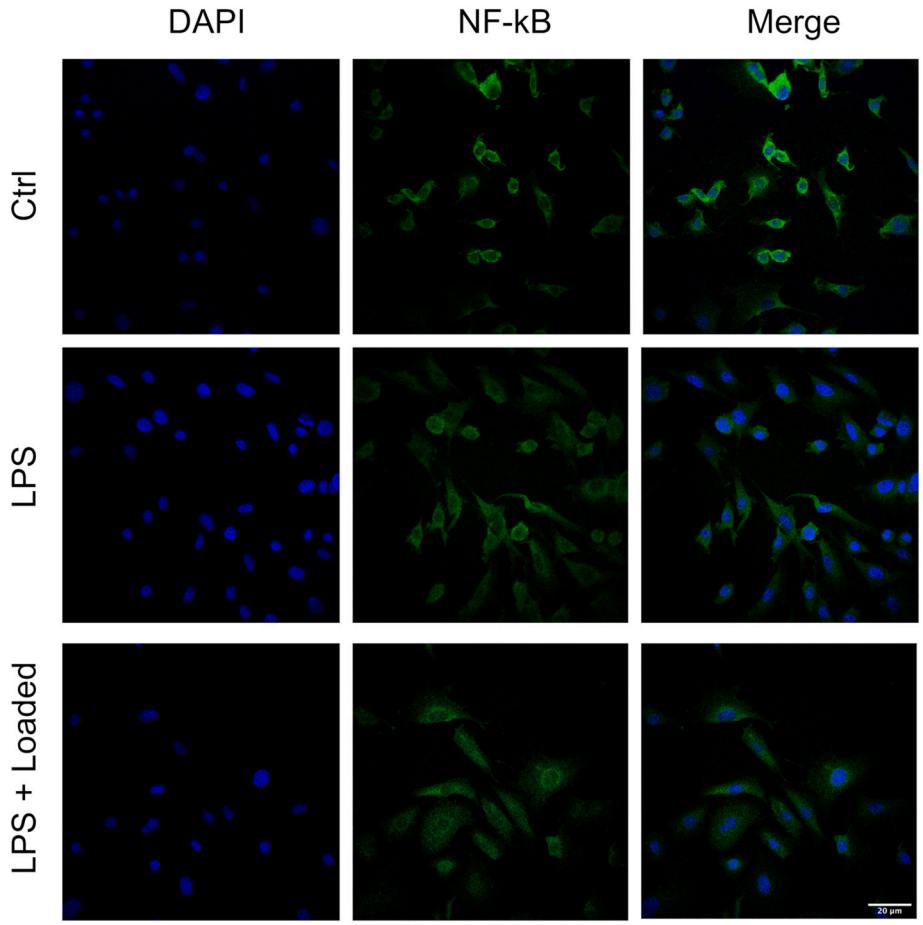

Fig. 7. Microscopy images of immunofluorescence labeling of NF-kB p65 (green) in 3T3-cells. LPS was used as a pro-inflammatory inducer. Cell treatment with nanovescicles prevents the nuclear translocation of p65 NF-kB.

1.43 with respect to dried ones (see Table 2). Furthermore, exudate penetration inside the fibres bundle has shown to be neglectable as the mean bundle area increases of a factor 1.30 after absorption. This different behaviour can be attributed to the different number of cells in the bundle and the quality of fibres that can be derived using different methods allowing the extraction of cellulose and non-cellulose compounds.

3.7. Wound-healing assay by quantitative phase imaging (QPI) analysis

Healing activity was evaluated by impregnating the Spanish broom dressing with extract, loaded, and unloaded ethosomes. It is widely reported that two essential processes must take place during wound healing: proliferation and cell migration [41]. Considering the absence of toxicity and the regular proliferation of fibroblasts, the scratch test

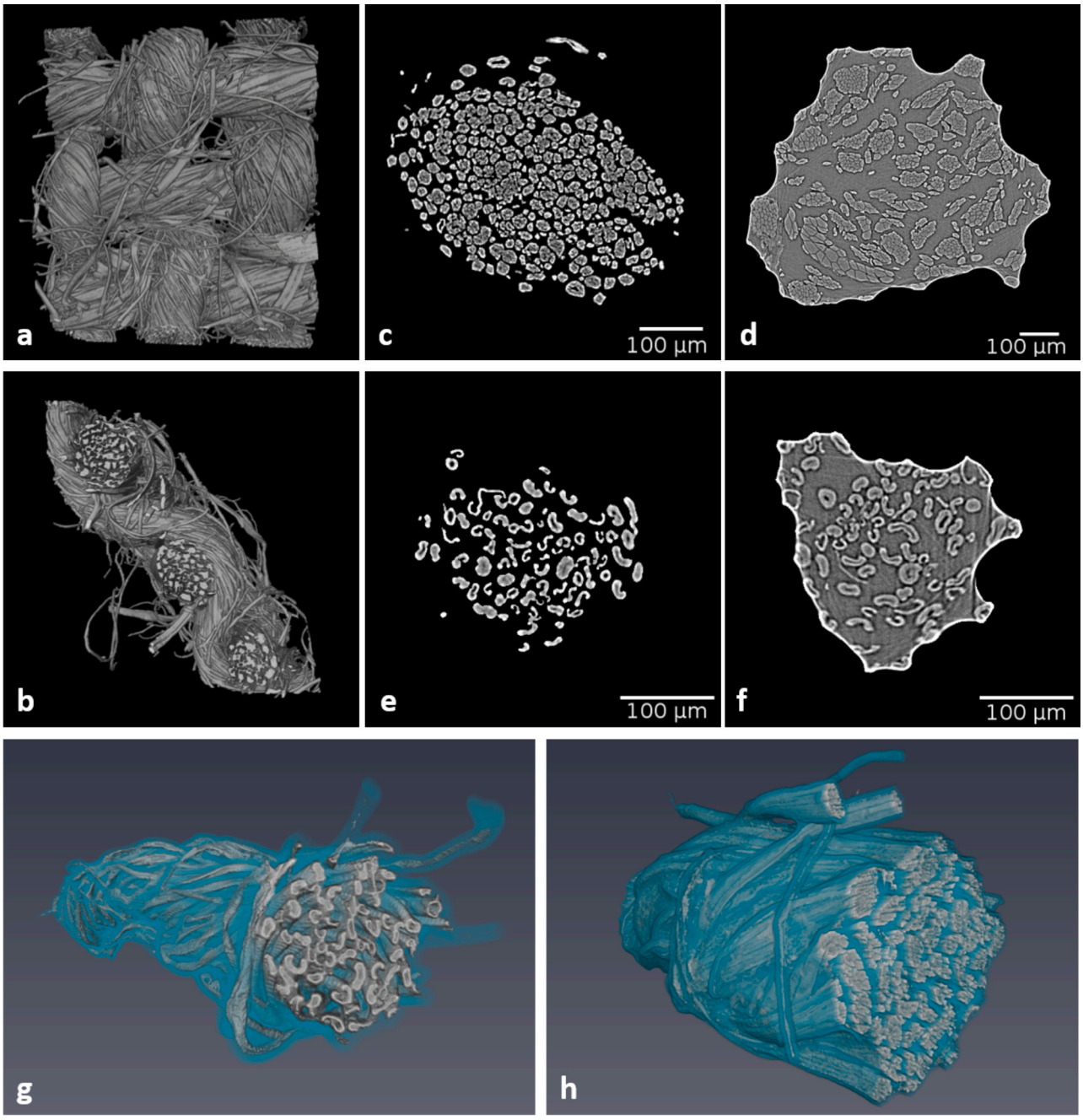

Fig. 8. Lateral (a) and frontal (b) views of 3D reconstruction of dried Spanish broom yarn (2 mm × 2.2 mm width and height). PCT axial view of dried Spanish broom fibres (c) and soaked (d). PCT axial view of dried cotton fibres (e) and soaked (f). 3D rendering of soaked cotton (g) and Spanish broom (h) bundles (length 2 mm), light blue colour highlights the exudate absorbed by the bundle.

Table 2
Cross-sectional bundles and fibres mean areas for Spanish broom and cotton fibres.

Sample	Cross-sectional bundle Area (μm^2)	Cross-sectional fibres Area (μm^2)
SB dry	105141 ± 6151	85062 ± 3492
SB wet	381549 ± 24,756	185816 ± 5286
Cotton dry	33266 ± 3249	13175 ± 1254
Cotton wet	43229 ± 3282	18615 ± 1780

was performed to assess collective cell migration in vitro.

The results showed that loaded ethosomes are able to reduce the healing time much more than the free extract and the unloaded ethosomes. After 48 h of treatments, the final formulation leads to complete closure of the scratch (Fig. 9 a, b). Indeed, the reduction in the time required to close half of the scratch and the highest cell speed support the effectiveness of the final formulation (Fig. 9 c, d), confirming the bioactive compounds such as polyphenols and saponins contained in *G. glabra* extract accelerate the entire healing process. In particular, polyphenols promote fibroblast proliferation and migration [42], and saponins promote vascular regeneration and shorten wound healing time [43].

4. Conclusions

Currently, the development of novel and effective wound dressings

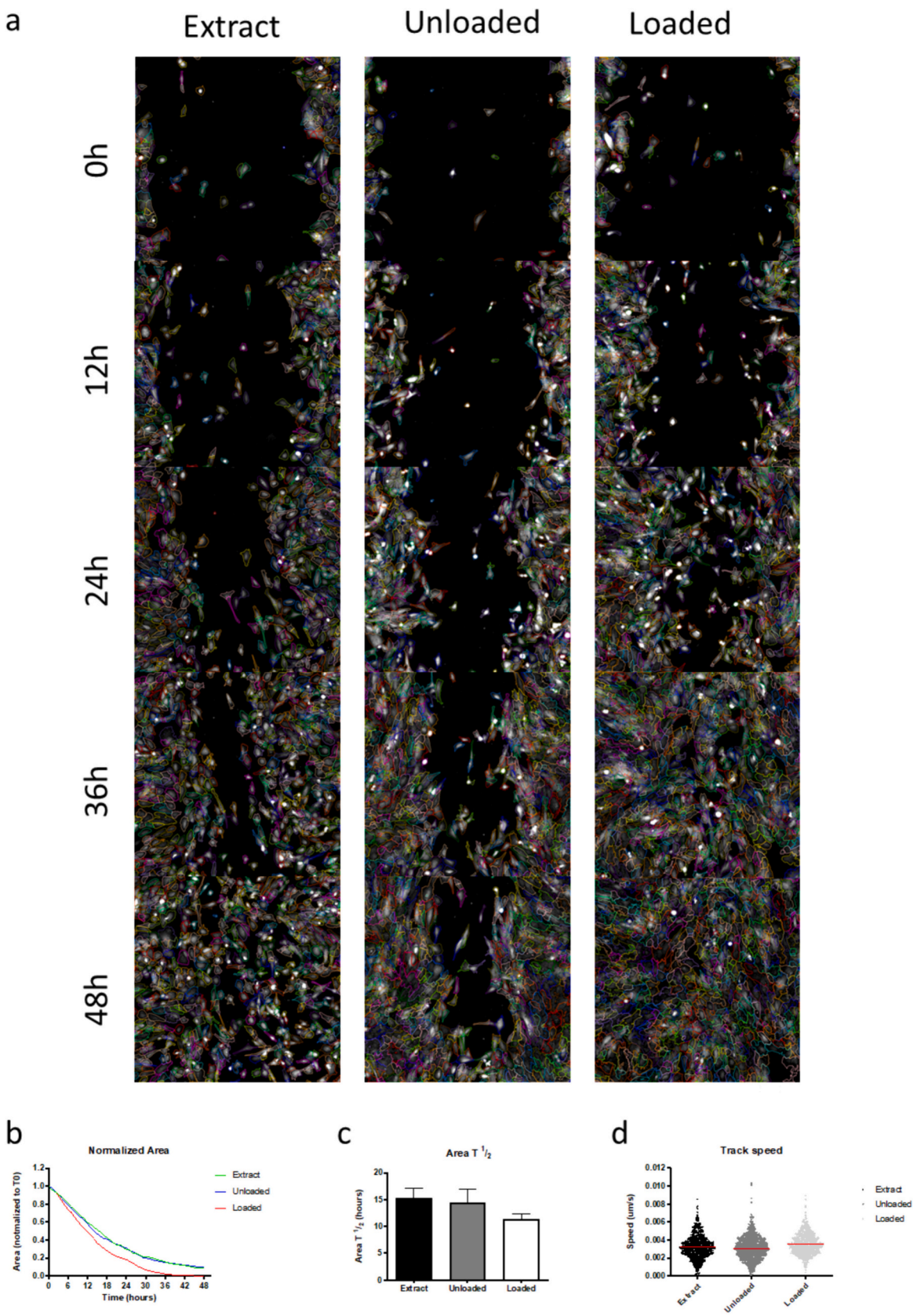

Fig. 9. Wound-healing effect of ethosomes and extract on 3T3 fibroblasts. (a) Quantitative phase imaging showing the area covered at 0, 12, 24, 36, and 48 h after wounding. Each image is representative of a scratch assay of the four experimental cell groups. Scale bar 100 μm. b) Area uncovered normalized to the initial time. c) Time in which ½ of the area was covered. d) A distribution plot of the track speed (μm/s), where track speed is defined as the total distance traveled divided by the total duration of the track.

remains a challenge for researchers worldwide. This work successfully developed an eco-sustainable wound dressing based on Spanish broom cellulose fibres impregnated with *G. glabra* extract-loaded ethosomes. *G. glabra* extract was encapsulated into ethosomes prepared by ethanol injection to preserve its biological activities. The lipid vesicles showed nanometric size, good entrapment efficiency, stability over time, and a sustained release of polyphenols that are crucial in promoting and accelerating wound healing. Moreover, biological studies showed that the extract encapsulated into ethosomes was highly biocompatible on fibroblasts and exhibited antioxidant and anti-inflammatory activity. The SR-PCmicroCT showed that Spanish broom cellulose fibres' appreciably absorbed exudates, making them suitable for wound treatment. Finally, Spanish broom wound dressing loaded with *G. glabra* ethosomes can accelerate wound closure, evidenced by the reduced wound healing time. In conclusion, the results of this study demonstrate the usefulness of natural biomaterials (Spanish broom fibres and *G. glabra* extract) in formulating novel, multifunctional, and eco-sustainable wound dressing. Further studies will be focused on the in vivo evaluation of the innovative formulation manufactured in this work.

CReDiT authorship contribution statement

Conceptualization, T.C., V.S.; methodology, V.S., M.R., M.M., C·C., L. M., E.M., E.L., M.F., G.T. and G.B.; validation, T.C., V.S., M.M., C.C.; investigation, V.S., M.R., A.D.B., M.A., F.R., M.M., I.C., C.C., M.P., E.L., M.F. and L.D.; data curation, T.C., V.S., M.R. and C.C.; writing—original draft preparation, T.C., V.S., M.R., C.C, L.M., E.L., M.F., G.T. and E.M.; writing—review and editing, T.C, V.S., C.C., M.M., A.A., B.L., and F.B.; supervision and project administration T.C.

All authors have read and agreed to the published version of the manuscript.

Funding

The project work was funded by the "Ministero dell'Università e della Ricerca": Development of sustainable and innovative Spanish Broom dressings containing Glycyrrhiza glabra L. and Spanish Broom extracts to heal skin wounds (SBresswound), PRIN 2022, project n. 2022JL9S9S CUP J53D23001100006.

Declaration of competing interest

The authors declare that they have no known competing financial interests or personal relationships that could have appeared to influence the work reported in this paper.

Data availability

Data will be made available on request.

Acknowledgments

The authors are thankful to Nicole Criniti for her contribution to the work. Martina Rossi is thankful University of Bologna for grant (Alma Idea 2022 CUP J45F21002000001).

References

[1] A.R. Khan, K. Huang, Z. Jinzhong, T. Zhu, Y. Morsi, A. Aldalbahi, M. El-Newehy, X. Yan, X. Mo, Colloids Surf. B Biointerfaces 196 (2020) 111352, https://doi.org/10.1016/j.colsurfb.2020.111352.
[2] D. Solanki, P. Vinchhi, M.M. Patel, ACS Omega 8 (9) (2023) 8172, https://doi.org/10.1021/acsomega.2c06806.
[3] Y. Liang, J. He, B. Guo, ACS Nano 15 (8) (2021) 12687, https://doi.org/10.1021/acsnano.1c04206.
[4] A. Eskandarinia, A. Kefayat, M. Gharakhloo, M. Agheb, D. Khodabakhshi, M. Khorshidi, V. Sheikhmoradi, M. Rafienia, H. Salehi, Int. J. Biol. Macromol. 149 (2020) 467–476, https://doi.org/10.1016/j.ijbiomac.2020.01.255.
[5] A. Kefayat, R. Hamidi Farahani, M. Rafienia, E. Hazrati, N., Hosseini Yekta, J. Iran. Chem. Soc. 19 (2022), https://doi.org/10.1007/s13738-021-02374-x, 1191–120.
[6] T. Cerchiara, G. Chidichimo, G. Rondi, M.C. Gallucci, C. Gattuso, B. Luppi, F. Bigucci, Fibres Text. East. Eur. 22 (2014) 25.
[7] T. Cerchiara, A. Abruzzo, R.A. Ñahui Palomino, B. Vitali, R. De Rose, G. Chidichimo, L. Ceseracciu, A. Athanassiou, B. Saladini, F. Dalena, F. Bigucci, B. Luppi, Eur. J. Pharm. Sci. 99 (2017) 105, https://doi.org/10.1016/j.ejps.2016.11.028.
[8] A. Abruzzo, C. Cappadone, G. Farruggia, B. Luppi, F. Bigucci, T. Cerchiara, Molecules 25 (2020) 2558, https://doi.org/10.3390/molecules25112558.
[9] T. Cerchiara, B. Giordani, L.M. Melgoza, C. Prata, C. Parolin, F. Dalena, A. Abruzzo, F. Bigucci, B. Luppi, B. Vitali, J. Drug Deliv. Sci. Technol. 56 (2020) 101499, https://doi.org/10.1016/j.jddst.2020.101499.
[10] T. Cerchiara, A. Abruzzo, M. di Cagno, F. Bigucci, A. Bauer-Brandl, C. Parolin, B. Vitali, M.C. Gallucci, B. Luppi, Eur. J. Pharm. Biopharm. 92 (2015) 112, https://doi.org/10.1016/j.ejpb.2015.03.004.
[11] J.-K. Kim, S. Oh, H.-S. Kwon, Y.-S. Oh, S.S. Lim, H.-K., Biochem. Biophys. Res. Commun. 345 (3) (2006) 1215, https://doi.org/10.1016/j.bbrc.2006.05.035.
[12] L. Shen, Z. Cui, Y. Lin, S. Wang, D. Zheng, Q. Tan, Burns 41 (2) (2015) 372, https://doi.org/10.1016/j.burns.2014.05.008.
[13] D.A. Safta, C. Bogdan, M.L. Moldovan, Pharmaceutics 14 (2022) 991, https://doi.org/10.3390/pharmaceutics14050991.
[14] V. Sallustio, I. Chiocchio, M. Mandrone, M. Cirrincione, M. Protti, G. Farruggia, A. Abruzzo, B. Luppi, F. Bigucci, L. Mercolini, F. Poli, T. Cerchiara, Molecules 27 (2022) 3025, https://doi.org/10.3390/molecules27093025.
[15] M. Balouiri, M. Sadiki, S.K. Ibnsouda, J. Pharm. Anal. 6 (2016) 71–79, https://doi.org/10.1016/j.jpha.2015.11.005.
[16] O. Tkachenko, J.A. Karas, J. Antimicrob. Chemother. 67 (7) (2012) 1697–1700, https://doi.org/10.1093/jac/dks110.
[17] X. Liu, H. Liu, J. Liu, Z. He, C. Ding, G. Huang, W. Zhou, L. Zhou, Int. J. Nanomedicine 6 (2011) 241, https://doi.org/10.2147/IJN.S16044.
[18] T. Uchino, F. Lefeber, G. Gooris, J. Bouwstra, Int. J. Pharm. 412 (2011) 142, https://doi.org/10.1016/j.ijpharm.2011.04.016.
[19] C. Dullin, F. di Lillo, A. Svetlove, J. Albers, W. Wagner, A. Markus, N. Sodini, D. Dreossi, F. Alves, G. Tromba, Phys. Open 6 (2021) 100050, https://doi.org/10.1016/j.physo.2020.100050.
[20] A. Bravin, P. Coan, P. Suortti, Phys. Med. Biol. 58 (1) (2013) R1–35, https://doi.org/10.1088/0031-9155/58/1/R1.
[21] I. Bukreeva, O. Junemann, A. Cedola, et al., J. Struct. Biol. 212 (3) (2020) 107659, https://doi.org/10.1016/j.jsb.2020.107659.
[22] T. Savi, A. Miotto, F. Petruzzellis, A. Losso, S. Pacilè, G. Tromba, S. Mayr, A. Nardini, Plant Physiol. Biochem. 120 (2017) 24, https://doi.org/10.1016/j.plaphy.2017.09.017.
[23] M. Tomasella, S. Natale, F. Petruzzellis, S. Di Bert, L. D'Amico, G. Tromba, A. Nardini, Plants 11 (2022) 307, https://doi.org/10.3390/plants11030307.
[24] C. Dullin, F. di Lillo, A. Svetlove, J. Albers, W. Wagner, A. Markus, N. Sodini, D. Dreossi, F. Alves, G. Tromba, Physics Open 6 (2021) 100050, https://doi.org/10.1016/j.physo.2020.100050.
[25] F. Brun, L. Massimi, M. Fratini, D. Dreossi, F. Billé, A. Accardo, R. Pugliese, A. Cedola, Adv. Struct. Chem. Imaging 3 (2017) 4, https://doi.org/10.1186/s40679-016-0036-8.
[26] B. Gabriele, T. Cerchiara, G. Salerno, G. Chidichimo, M.V. Vetere, C. Alampi, M. C. Gallucci, C. Conidi, A. Cassano, Bioresour. Technol. 101 (2010) 724, https://doi.org/10.1016/j.biortech.2009.08.014.
[27] L. Ripoll, C. Bordes, S. Etheve, A. Elaissari, H. Fessi, E-Polymers 40 (2010) 1, https://doi.org/10.1515/epoly.2010.10.1.409.
[28] H. Hayashi, H. Sudo, Plant Biotechnology 26 (1) (2009) 101, https://doi.org/10.5511/plantbiotechnology.26.101.
[29] G. Pastorino, L. Cornara, S. Soares, F. Rodrigues, M.B.P.P. Oliveira, Phytother. Res. 32 (12) (2018) 2323, https://doi.org/10.1002/ptr.6178.
[30] S. Ercisli, I. Coruh, A. Gormez, M. Sengul, S. Bilena, Ital J Food Sci 20 (1) (2008) 91.
[31] T.K. Lim, *Glycyrrhiza glabra*, in: Edible Medicinal and Non-Medicinal Plants, Springer Netherlands, Dordrecht, 2016, pp. 354–457, https://doi.org/10.1007/978-94-017-7276-1_18.
[32] F. Karahan, C. Avsar, I.I. Ozyigit, I. Berber, Biotechnol. Biotechnol. Equip. 30 (4) (2016) 797–804, https://doi.org/10.1080/13102818.2016.1179590.
[33] CLSI, Methods for Determining Bactericidal Activity of Antimicrobial Agents. Approved Guideline, CLSI Document M26-a. Clinical and Laboratory Standards Institute, 950 West Valley Roadn Suite 2500, Wayne, Pennsylvania 19087, USA, 1998.
[34] R.-D. Păvăloiu, F. Sha'at, C. Bubueanu, M. Deaconu, G. Neagu, M. Sha'at, M. Anastasescu, M. Mihailescu, C. Matei, G. Nechifor, et al., Nanomaterials 10 (2020) 56, https://doi.org/10.3390/nano10010056.
[35] K. Makino, T. Yamada, M. Kimura, T. Oka, H. Ohshima, T. Kondo, Biophys. Chem. 41 (2) (1991) 175, https://doi.org/10.1016/0301-4622(91)80017-L.
[36] R.-D. Păvăloiu, F. Sha'at, G. Neagu, M. Deaconu, C. Bubueanu, A. Albulescu, M. Sha'at, C. Hlevca, Nanomaterials, 11 (2021) 1938. doi:https://doi.org/10.3390/nano11081938.
[37] R. Gharib, A. Amal Najjar, L. Auezova, C. Catherine Charcosset, H. Greige-Gerges, J. Membrane Biol. 250 (2017) 259, https://doi.org/10.1007/s00232-017-9957-y.
[38] R. Kumar, et al., Med. Oncol. 40 (2023) 169, https://doi.org/10.1007/s12032-023-02035-4.
[39] Santos et al. Biol. Sex Differ. (2017) 8:30 DOI https://doi.org/10.1186/s13293-017-0151-9.

[40] B. Azimi, H. Maleki, L. Zavagna, J.G. De la Ossa, S. Linari, A. Lazzeri, S. Danti, J. Funct. Biomater. 11 (2020) 67, https://doi.org/10.3390/jfb11030067.
[41] A.M. Wojtowicz, S. Oliveira, M.W. Carlson, A. Zawadzka, C.F. Rousseau, D. Baksh, Wound Repair Regen. 22 (2) (2014) 246, https://doi.org/10.1111/wrr.12154.
[42] I. Guimarães, S. Baptista-Silva, M. Pintado, A.L. Oliveira, Appl. Sci. 11 (2021) 1230, https://doi.org/10.3390/app11031230.
[43] E. Liu, H. Gao, Y. Zhao, Y. Pang, Y. Yao, Z. Yang, X. Zhang, Y. Wang, S. Yang, X. Ma, J. Zeng, J. Guo, Front. Pharmacol. 13 (2022) 900439, https://doi.org/10.3389/fphar.2022.900439.